Extended lattice Boltzmann method for numerical simulation of thermal phase change in two-phase fluid flow

Hesameddin Safari,[1,2] Mohammad Hassan Rahimian,[1] and Manfred Krafczyk[2]
[1]*Department of Mechanical Engineering, College of Engineering, University of Tehran, Tehran, Iran*
[2]*Institute for Computational Modeling in Civil Engineering, Technische Universität Braunschweig, Braunschweig, Germany*
(Received 19 February 2013; published 8 July 2013)

In this article, a method based on the multiphase lattice Boltzmann framework is presented which is applicable to liquid-vapor phase-change phenomena. Both liquid and vapor phases are assumed to be incompressible. For phase changes occurring at the phase interface, the divergence-free condition of the velocity field is no longer satisfied due to the gas volume generated by vaporization or fluid volume generated by condensation. Thus, we extend a previous model by a suitable equation to account for the finite divergence of the velocity field within the interface region. Furthermore, the convective Cahn-Hilliard equation is extended to take into account vaporization effects. In a first step, a D1Q3 LB model is constructed and validated against the analytical solution of a one-dimensional Stefan problem for different density ratios. Finally the model is extended to two dimensions (D2Q9) to simulate droplet evaporation. We demonstrate that the results obtained by this approach are in good agreement with theory.

DOI: 10.1103/PhysRevE.88.013304 PACS number(s): 47.11.−j, 47.55.−t, 64.70.fm, 44.35.+c

I. INTRODUCTION

Two-phase gas-liquid flows including phase changes play an important role in many natural processes such as the weather (e.g., fog or evaporation of water across the soil-atmosphere interface) as well as in industrial applications such as combustion engines, heat exchangers, boilers, dryers, etc. Experimental investigations as well as numerical simulations will lead to better understanding of these systems. Due to the potential multitude of the relevant spatial and temporal scales of phase-change processes, one frequently encounters technical barriers to obtaining accurate experimental measurements. The development of numerical methods to be validated by preliminary experimental measurements is a powerful complementary approach to gain in-depth insight into the fundamental physics of phase change in vapor-liquid flows (i.e., boiling, evaporation, and condensation).

Different methods for the direct numerical simulation of gas-liquid flows including phase changes have been presented over the past decades. For Navier-Stokes solvers, the volume of fluid method [1], the level set method [2], and front tracking methods [3] are the most common numerical strategies to describe the dynamics of the phase interface. Despite the growing body of research on the aforementioned flows, the direct simulation of two-phase flows with (reactive) dynamic interfaces is still a challenging task. The major difficulties are due to the coupling of many effects such as interfacial mass transfer, latent heat, and surface tension in accordance with the relevant conservation laws of mass, momentum, and energy.

The lattice Boltzmann method (LBM) which is based on mesoscopic kinetic equations seems to be a promising method for dealing with interfacial flows. The mesoscopic nature of LBM aims to include only a minimum amount of microscopic details to reproduce interfacial physics and macroscopic flow hydrodynamics in a consistent manner. Therefore, it can address length scales between macroscale and microscale and simulate phase interfaces from a more fundamental basis.

During the last decades, various lattice Boltzmann (LB) models have been proposed for simulation of complex fluids, especially multiphase and multicomponent flows. The earlier LB models of multiphase flows had many drawbacks when applying them to practical problems such as stability problems for high density and viscosity ratios as well as large spurious currents in the vicinity of the interface due to inconsistencies in the numerical discretization of different parts of the pressure tensor. During the last decade different strategies have been proposed to cure the aforementioned deficiencies [4–6]. In spite of many successes that have been achieved by modern LB multiphase models, the thermodynamically consistent simulation of thermal phase changes in a gas-liquid system has rarely been addressed in the LBM related literature. Many physical problems such as rising bubbles, falling droplets, droplet coalescence, wall wetting, and contact line dynamics have been simulated with different LB models to date. Yet, a comprehensive study of thermal phase-change phenomena based on thermodynamically consistent LBM approaches seems to be lacking.

One of the first attempts in this field can be found in Palmer and Rector [7]. They incorporated thermal effects in a two-phase lattice Boltzmann framework and used the free-energy model of Swift *et al.* [8] in combination with an internal energy distribution function thermal model and solved some simple examples such as evaporation of a thin liquid film from a heated plate and evaporation of an isolated droplet. Later they pointed out that an error in reducing the data from some of their simulations had caused them to conclude that the algorithm could consistently model evaporation of a fluid [9]. Their further analysis proved that their LBM algorithm cannot be used for quantitative simulations of evaporation or other thermally driven phase changes.

Lee and Lin proposed a pressure evolution equation LBM formulation for an isothermal two-phase fluid flow with phase changes [10]. The pressure evolution equation was derived by taking into account the time derivative of the equation of state for nonideal gases. This model permits compressibility of the fluid at phase interfaces when phase change occurs due to pressurization and depressurization. They applied the model to simulate a one-dimensional isothermal

phase-change process and their results were in good agreement with analytical solutions. According to the first author's private communications with Lee, this model has not been further developed and extended to two-dimensional and more practical cases because of its limited stability.

Zhang and Chen presented a pseudopotential model (based on the approach by Shan-Chen), capable of simulating thermal multiphase flows [11]. They claimed that their approach is thermodynamically consistent at the macroscopic level. The evolution of temperature was modeled by solving the scalar energy transport equation with a finite difference scheme. The liquid-vapor boiling process, including liquid-vapor formation and coalescence together with a coupling of temperature, was simulated. Yet, only qualitative results were reported and no validation or quantitative comparisons with experimental or analytical data were provided. Instead, the authors listed necessary improvements for further studies including a more physical treatment of the heat capacity and latent heat, incorporation of more realistic equations of state (EOS) instead of the van der Waals EOS, improvement with respect to numerical stability to achieve significantly higher density ratio and lower viscosity, and comparisons with experimental results.

Dong *et al.* [12] combined the multiphase LBM of Zheng *et al.* [13] with a passive scalar LB thermal model to investigate the growth and deformation of a rising vapor bubble in a superheated liquid. In the multiphase model of Zheng *et al.* the convective Cahn-Hilliard equation is employed for interface capturing. However, it has been demonstrated that Zheng's model is only valid for uniform densities and its application for large density ratios is questionable [14]. Dong *et al.* used a passive scalar approach for evaluating the temperature variations and a separate distribution function was employed for recovering the heat equation. In their model the phase change is considered as a change of phase order parameter and a source term was added to the Cahn-Hilliard equation. Later in 2010, they employed this model to simulate bubble growth on and departure from a superheated wall [15]. Their modeling approach has two main drawbacks. First, the application of Zheng's model to problems with high density ratios is not consistent. Secondly, they only added a source term to the Cahn-Hilliard equation to track the interface, but the momentum equation remained unchanged. This means that the phase-change process only moves the interface location without any velocity change in the computational domain. Physically the process of phase change should induce a net momentum into the flow field which has not been considered in their model.

Márkus and Házi [16] have improved the model of Zhang and Chen [11] and performed a quantitative analysis. They improved the discretization of interparticle potential force in order to increase stability. A passive scalar thermal LBM has been incorporated in their model. They utilized macroscopic jump conditions to evaluate the accuracy of their results for the one-dimensional problem of evaporation through a plane-phase interface. They also extended the model to two dimensions and investigated heterogeneous boiling. Based on their results, important features of the boiling process could be captured qualitatively by this model.

It seems that two different approaches can be employed for simulation of phase-change process in a two-phase fluid flow. One can model the phase transition in a thermodynamically consistent manner which means that the nonideal gas equation of state (EOS) governs the equilibrium state between liquid and vapor phases, respectively. In this context, the change in pressure or temperature alters the equilibrium and the phase transition will be automatically controlled via the equation of state. Most of the LBMs discussed above belong to this category [7,10,11,16].

Another approach is similar to the idea which is incorporated in the volume of fluid (VOF), level set, and some other front tracking methods for phase-change modeling. In this concept the gas and liquid phases are considered as an immiscible and incompressible fluid system. The mass transfer rate through the interface is estimated by a suitable correlation related to the temperature gradient or vapor mass fraction (species concentration) gradient. One example of such an LBM framework is the work of Dong *et al.* [12]. However, their formalism and results have problems as discussed above.

In addition to partial inconsistencies such as neglecting volumetric changes at the interfaces due to phase changes, according to our test, the models described above suffer from numerical instability at high density and viscosity ratios which limits their applications in most practical cases.

Recently Lee proposed a remarkable lattice Boltzmann multiphase scheme based on the Cahn-Hilliard diffuse interface theory [17] which overcomes most of the limitations which previous LB multiphase models faced. As a result of using the potential form of the intermolecular force for nonideal fluids and compact isotropic discretization of this forcing term, spurious currents could be reduced to round-off and stable solutions are obtained for density ratios up to 1:1000, at least for low Mach numbers. Recently Li *et al.* [18] have shown that LB Cahn-Hilliard-like interface capturing methods contain an additional force term in the recovered momentum equation. The force has zero value in bulk phases but nonzero across the interface, so it can be considered as an additional interfacial force. The effects of this unwanted interfacial force become more significant when the velocity or the Reynolds number increases.

In this paper, the binary-fluid model of Lee is extended to simulate thermal phase-change phenomena in two-phase fluid flows. Both liquid and gas phases are considered to be incompressible. However, the phase-change process is modeled by incorporating a proper source term at the phase interface. First the extension of the classical convective Chan-Hilliard equation in the presence of phase change is presented. Then this modified evolution equation is employed in the multiphase LB framework of Lee. The developed model is successfully validated for a one-dimensional Stefan problem with different density ratios up to 1:1000. Finally the ability of the model to simulate two-dimensional droplet evaporation is tested.

II. MATHEMATICAL MODELING

A. Extension of convective Cahn-Hilliard equations

Consider the system of two incompressible and immiscible fluids of different bulk density (i.e., ρ_l as liquid phase density and ρ_g as gas phase density). Similar to the volume of

fluid (VOF) method, the two phases are distinguished by their composition in a volume element of the domain. This composition C takes a value of 1 in the liquid phase and a lower value in the gas phase ($0 \leqslant C \leqslant 1$). So the local densities ($\tilde{\rho}_i$) are related to bulk densities (ρ_I) by

$$\tilde{\rho}_l = C\rho_l, \quad \tilde{\rho}_g = (1-C)\,\rho_g. \tag{1}$$

The local averaged density is denoted by $\rho = C\rho_l + (1-C)\,\rho_g$.

The continuity equation for component i may be written as

$$\frac{\partial \tilde{\rho}_i}{\partial t} + \nabla \cdot \mathbf{n}_i = \pm \dot{m}''' \quad (i = l, g), \tag{2}$$

where $\mathbf{n}_i$ is the mass flow rate (per unit volume) of the component i and $\dot{m}'''$ denotes the volumetric source or sink due to phase changes. In the bulk region, the mass flow is only attributed to advection, thus $\mathbf{n}_i = \tilde{\rho}_i \mathbf{u}$ where $\mathbf{u}$ is the volume averaged velocity of the flow. In interfacial regions, a diffusive flow may exist as a result of the smooth transition of the composition between the different phases. This diffusive mass flow is indicated by $-\rho_i \mathbf{j}_i$, where $\mathbf{j}_i$ is the volume diffusive flow rate. Thus the total mass flow rate of component i is expressed as [19]

$$\mathbf{n}_i = \tilde{\rho}_i \mathbf{u} - \rho_i \mathbf{j}_i. \tag{3}$$

Equation (2) can be written in terms of C for each phase by recalling Eq. (1):

$$\frac{\partial C}{\partial t} + \nabla \cdot (\mathbf{u}C) - \nabla \cdot \mathbf{j}_l = -\frac{\dot{m}'''}{\rho_l} \quad \text{for the liquid phase, and} \tag{4}$$

$$\frac{\partial (1-C)}{\partial t} + \nabla \cdot [\mathbf{u}(1-C)] - \nabla \cdot \mathbf{j}_g = \frac{\dot{m}'''}{\rho_g} \quad \text{for the gas phase.} \tag{5}$$

If the diffusive flow rate is only related to compositions [19], $\mathbf{j}_l = -\mathbf{j}_g = \mathbf{j}$. Thus, the divergence of velocity field can be obtained from Eqs. (4) and (5):

$$\nabla \cdot \mathbf{u} = \dot{m}''' \left(\frac{1}{\rho_g} - \frac{1}{\rho_l} \right). \tag{6}$$

Note that in the absence of any phase change, the volumetric source vanishes and the divergence-free condition of the velocity field will be satisfied.

Cahn and Hilliard assumed that the diffusive flow rate is proportional to the gradient of chemical potential [17], say $\mathbf{j} = M\nabla\mu$ where $M > 0$ is the mobility. They related the mixing energy density of an isothermal system to composition by $E_{\text{mix}}(C, \nabla C) = E_0(C) + \kappa |\nabla C|^2/2$, where $E_0 = \beta C^2 (1-C)^2$ is the bulk energy. The derivative of E_0 with respect to C gives the classical part of the chemical potential, i.e., $\mu_0 = \partial_C E_0$. The equilibrium profile between two phases may be obtained by minimizing the mixing energy. This will lead to the following equation for the chemical potential μ which is used to determine the diffusive flow rate:

$$\mu = \mu_0 - \kappa \nabla^2 C. \tag{7}$$

For a detailed explanation about mixing energy and parameters such as κ and β, see [6,17].

Finally the behavior of the binary-fluids system is governed by the transport equation of composition C as

$$\frac{\partial C}{\partial t} + \nabla \cdot (\mathbf{u}C) = \nabla \cdot (M \nabla \mu) - \frac{\dot{m}'''}{\rho_l}. \tag{8}$$

In the case of zero volumetric source term, $\nabla \cdot \mathbf{u}$ and $\dot{m}'''$ vanish and Eq. (8) reduces to the classical convective Cahn-Hilliard equation. The calculation of $\dot{m}'''$ will be presented later.

B. Lattice Boltzmann equations for the flow field

By incorporating the intermolecular interaction force, the discrete Boltzmann equation (DBE) for the transport of density and momentum of a nonideal fluid can be written as [17]

$$\frac{Df_\alpha}{Dt} = \frac{\partial f_\alpha}{\partial t} + \mathbf{e}_\alpha \cdot \nabla f_\alpha = -\frac{1}{\lambda}\left(f_\alpha - f_\alpha^{eq}\right) + \frac{1}{\rho c_s^2}(\mathbf{e}_\alpha - \mathbf{u}) \cdot \mathbf{F} f_\alpha^{eq}, \tag{9}$$

where f_α are the particle distribution functions, $\mathbf{e}_\alpha$ is the microscopic particle velocity with discrete index α, ρ is the density, $\mathbf{u}$ is the volume averaged velocity, c_s^2 is the speed of sound, λ is the relaxation time, and f_α^{eq} is the equilibrium distribution function:

$$f_\alpha^{eq} = w_\alpha \rho \left[1 + \frac{\mathbf{e}_a \cdot \mathbf{u}}{c_s^2} + \frac{(\mathbf{e}_a \cdot \mathbf{u})^2}{2c_s^4} - \frac{(\mathbf{u} \cdot \mathbf{u})}{2c_s^2} \right], \tag{10}$$

where w_α is the weight factor determined from lattice structure. The external force $\mathbf{F}$ representing the intermolecular interaction and nonideal gas effects can be expressed as

$$\mathbf{F} = \nabla \rho c_s^2 - \nabla p_{th} + \rho \kappa \nabla \nabla^2 \rho, \tag{11}$$

where p_{th} is the thermodynamic pressure and $\rho\kappa\nabla\nabla^2\rho$ is responsible for surface tension effects. Equation (11) is the pressure form of the external force. Lee [17] has shown that by employing the potential form of the external force instead of the pressure form and higher-order finite difference treatment, parasitic currents are tamed substantially. For binary fluids, the external force $\mathbf{F}$ is computed by replacing the density by the composition C and taking the free energy of the system into account. Furthermore, Lee included the hydrodynamic pressure (p_h) gradient to the forcing term which enforces incompressibility:

$$\mathbf{F} = \nabla \rho c_s^2 - \nabla p_h - C \nabla \mu. \tag{12}$$

The total pressure can be assumed as the sum of the thermodynamic pressure, the hydrodynamic pressure, and the pressure contribution due to curvature of the phase interface [17]:

$$p_{tot} = p_{th} + p_h - \kappa C \nabla^2 C + \tfrac{1}{2}\kappa |\nabla C|^2. \tag{13}$$

The DBE of Eq. (9) evolves the density and momentum. One can evolve the pressure instead of the density by introducing a new distribution function as

$$g_\alpha = f_\alpha c_s^2 + \left(p_h - \rho c_s^2\right) \Gamma_\alpha(0), \tag{14}$$

where $\Gamma_\alpha(\mathbf{u}) = \frac{f_\alpha^{eq}}{\rho}$. The DBE of the new distribution function g_α can be found by taking the total derivative of Eq. (14):

$$\frac{Dg_\alpha}{Dt} = c_s^2 \frac{Df_\alpha}{Dt} + \left(\frac{Dp_h}{Dt} - c_s^2 \frac{D\rho}{Dt} \right) \Gamma_\alpha(0). \tag{15}$$

The total derivative is expressed as $D_t() = \partial_t() + e_\alpha \cdot \nabla()$. Lee assumed the divergence-free condition of the velocity field and by using the continuity equation [i.e., $\partial_t(\rho) + \nabla \cdot (\rho \mathbf{u}) = 0$], the total derivatives of Eq. (15) can be stated as

$$\frac{D\rho}{Dt} = (\mathbf{e}_\alpha - \mathbf{u}) \cdot \nabla \rho, \quad \frac{Dp_h}{Dt} = (e_\alpha - \mathbf{u}) \cdot \nabla p_h. \tag{16}$$

When phase change occurs at the interface, the divergence-free condition of the velocity is no longer satisfied. Thus the total derivatives of Eq. (16) will be changed. For simplicity we assume that the phase change has no effect on the incompressibility of two phases and does not affect the hydrodynamic pressure, but density would be changed due to phase transition. Hence the total derivative of the hydrodynamic pressure remains the same as Eq. (16) and by combining the continuity equation and Eq. (6), the total derivative of the density can be computed as

$$\begin{aligned}\frac{D\rho}{Dt} &= (\mathbf{e}_\alpha - \mathbf{u}) \cdot \nabla \rho - \rho \nabla \cdot \mathbf{u} \\ &= (\mathbf{e}_\alpha - \mathbf{u}) \cdot \nabla \rho - \dot{m}''' \rho \left(\frac{1}{\rho_g} - \frac{1}{\rho_l} \right). \end{aligned} \tag{17}$$

Finally the DBE for the evolution of the hydrodynamic pressure and momentum is as follows:

$$\begin{aligned}\frac{\partial g_\alpha}{\partial t} + e_\alpha \cdot \nabla g_a = &-\frac{1}{\lambda} \left(g_\alpha - g_\alpha^{eq} \right) + (\mathbf{e}_\alpha - \mathbf{u}) \\ &\cdot \left\{ \nabla \rho c_s^2 \left[\Gamma_\alpha - \Gamma_\alpha(0) \right] - C \nabla \mu \Gamma_\alpha \right\} \\ &+ \rho c_s^2 \dot{m}''' \left(\frac{1}{\rho_g} - \frac{1}{\rho_l} \right) \Gamma_\alpha(0), \end{aligned} \tag{18}$$

where the new equilibrium distribution function is

$$\begin{aligned} g_\alpha^{eq} &= f_\alpha^{eq} c_c^2 + \left(p_h - \rho c_c^2 \right) \Gamma_\alpha(0) \\ &= w_\alpha \left\{ p_h + \rho c_c^2 \left[\frac{\mathbf{e}_a \cdot \mathbf{u}}{c_s^2} + \frac{(\mathbf{e}_a \cdot \mathbf{u})^2}{2c_s^4} - \frac{(\mathbf{u} \cdot \mathbf{u})}{2c_s^2} \right] \right\}. \end{aligned} \tag{19}$$

In the derivation of Eq. (18), the gradient of hydrodynamic pressure is neglected. This is due to the fact that in low Mach number flows the hydrodynamic pressure is assumed to be $p_h \approx O(Ma^2)$, so the gradient term $(e_a - u) \cdot \nabla p_h [\Gamma_\alpha - \Gamma_\alpha(0)] \approx O(Ma^3)$ can be neglected.

The lattice Boltzmann equation (LBE) of Eq. (18) is derived by applying a trapezoidal integration along characteristics over time step δt as:

$$\begin{aligned} &\bar{g}_\alpha(\mathbf{x} + \mathbf{e}_\alpha \delta t, t + \delta t) - \bar{g}_\alpha(\mathbf{x}, t) \\ &= -\frac{1}{\tau + 0.5} \left(\bar{g}_\alpha - \bar{g}_\alpha^{eq} \right) \Big|_{(\mathbf{x},t)} + \delta t (\mathbf{e}_\alpha - \mathbf{u}) \\ &\quad \cdot \left\{ \nabla \rho c_s^2 \left[\Gamma_\alpha - \Gamma_\alpha(0) \right] - C \nabla \mu \Gamma_\alpha \right\}_{(\mathbf{x},t)} \\ &\quad + \frac{\delta t}{2} \rho c_s^2 \dot{m}''' \left(\frac{1}{\rho_g} - \frac{1}{\rho_l} \right) \Gamma_\alpha(0) \Big|_{(\mathbf{x},t)} \\ &\quad + \frac{\delta t}{2} \rho c_s^2 \dot{m}''' \left(\frac{1}{\rho_g} - \frac{1}{\rho_l} \right) \Gamma_\alpha(0) \Big|_{(\mathbf{x}+\mathbf{e}_\alpha \delta t, t+\delta t)}, \end{aligned} \tag{20}$$

where $\tau = \lambda / \delta t$ is the nondimensional relaxation time. $\bar{g}_\alpha$ and $\bar{g}_\alpha^{eq}$ are particle and equilibrium distribution functions which are defined to retain the scheme as an explicit one with second-order accuracy.

$$\begin{aligned} \bar{g}_\alpha &= g_\alpha + \frac{\left(g_\alpha - g_\alpha^{eq} \right)}{2\tau} \\ &\quad - \frac{\delta t}{2} (\mathbf{e}_\alpha - \mathbf{u}) \cdot \left\{ \nabla \rho c_s^2 \left[\Gamma_\alpha - \Gamma_\alpha(0) \right] - C \nabla \mu \Gamma_\alpha \right\}, \end{aligned} \tag{21}$$

$$\bar{g}_\alpha^{eq} = g_\alpha^{eq} - \frac{\delta t}{2} (\mathbf{e}_\alpha - \mathbf{u}) \cdot \left\{ \nabla \rho c_s^2 \left[\Gamma_\alpha - \Gamma_\alpha(0) \right] - C \nabla \mu \Gamma_\alpha \right\}. \tag{22}$$

A new distribution function is needed for evolution of the composition C. It should recover the extended convective Cahn-Hilliard equation [Eq. (8)]. One of the simplest choices for particle and equilibrium distribution functions are $h_\alpha = (C/\rho) f_\alpha$ and $h_\alpha^{eq} = (C/\rho) f_\alpha^{eq}$ respectively. The DBE for the transport of the composition can be obtained by taking the total derivative of h_α. From Eqs. (6) and (8), the total derivative of the composition C is written as

$$\frac{DC}{Dt} = (\mathbf{e}_\alpha - \mathbf{u}) \cdot \nabla C - C \nabla \cdot \mathbf{u} + \nabla \cdot (M \nabla \mu) - \frac{\dot{m}'''}{\rho_l}. \tag{23}$$

The DBE for h_α can be written in the following form:

$$\begin{aligned} \frac{\partial h_\alpha}{\partial t} + e_\alpha . \nabla h_a = &-\frac{1}{\lambda} \left(h_\alpha - h_\alpha^{eq} \right) + (\mathbf{e}_\alpha - \mathbf{u}) \\ &\cdot \left[\nabla C - \frac{C}{\rho c_s^2} (\nabla p_h + C \nabla \mu) \right] \Gamma_\alpha \\ &+ \left(M \nabla^2 \mu - \frac{\dot{m}'''}{\rho_l} \right) \Gamma_\alpha. \end{aligned} \tag{24}$$

By applying a trapezoidal integration along characteristics over time step δt we obtain the following LBE:

$$\begin{aligned} &\bar{h}_\alpha(\mathbf{x} + \mathbf{e}_\alpha \delta t, t + \delta t) - \bar{h}_\alpha(\mathbf{x}, t) \\ &= -\frac{1}{\tau + 0.5} \left(\bar{h}_\alpha - \bar{h}_\alpha^{eq} \right) \Big|_{(\mathbf{x},t)} \\ &\quad + \delta t (\mathbf{e}_\alpha - \mathbf{u}) \cdot \left[\nabla C - \frac{C}{\rho c_s^2} (\nabla p_h + C \nabla \mu) \right] \Gamma_\alpha \Big|_{(\mathbf{x},t)} \\ &\quad + \frac{\delta t}{2} \left(M \nabla^2 \mu - \frac{\dot{m}'''}{\rho_l} \right) \Gamma_\alpha \Big|_{(\mathbf{x},t)} \\ &\quad + \frac{\delta t}{2} \left(M \nabla^2 \mu - \frac{\dot{m}'''}{\rho_l} \right) \Gamma_\alpha \Big|_{(\mathbf{x}+\mathbf{e}_\alpha \delta t, t+\delta t)}, \end{aligned} \tag{25}$$

where the modified distribution functions $\bar{h}_\alpha$ and $\bar{h}_\alpha^{eq}$ are defined as follows:

$$\begin{aligned} \bar{h}_\alpha &= h_\alpha + \frac{\left(h_\alpha - h_\alpha^{eq} \right)}{2\tau} \\ &\quad - \frac{\delta t}{2} (\mathbf{e}_\alpha - \mathbf{u}) \cdot \left[\nabla C - \frac{C}{\rho c_s^2} (\nabla p_h + C \nabla \mu) \right] \Gamma_\alpha, \end{aligned} \tag{26}$$

$$\bar{h}_\alpha^{eq} = h_\alpha^{eq} - \frac{\delta t}{2} (\mathbf{e}_\alpha - \mathbf{u}) \cdot \left[\nabla C - \frac{C}{\rho c_s^2} (\nabla p_h + C \nabla \mu) \right] \Gamma_\alpha. \tag{27}$$

The gradient terms of Eqs. (20)–(22) and (25)–(27) are discretized in accordance with Lee's suggestions [6,20].

It should be noted that in Eqs. (20) and (25) the last term on the right-hand-side is approximated at $(\mathbf{x}+\mathbf{e}_\alpha\delta t,t)$ instead of $(\mathbf{x}+\mathbf{e}_\alpha\delta t,t+\delta t)$ in order to avoid implicitness in C and T. As mentioned by Lee and Liu [20], this approximation does not violate the second-order accuracy of the scheme.

The composition, hydrodynamic pressure, and momentum are calculated by taking the zero- and first-order moments of the modified distribution function:

$$C=\sum_\alpha \bar{h}_\alpha, \tag{28}$$

$$\rho\mathbf{u}=\frac{1}{c_s^2}\sum_\alpha \mathbf{e}_\alpha\bar{g}_\alpha-\frac{\delta t}{2}C\nabla\mu, \tag{29}$$

$$p_h=\sum_\alpha \bar{g}_\alpha+\frac{\delta t}{2}\mathbf{u}\cdot\nabla\rho c_s^2. \tag{30}$$

C. Lattice Boltzmann equations for temperature field

Since the focus of this paper is on the proper phase-change modeling in low Mach number and incompressible limits of the fluid flow, the pressure work and heat dissipation could be ignored. Hence, the simple passive scalar approach is employed for the evolution of the temperature field in the computational domain. In this approach the temperature is passively advected by a fluid velocity and the coupling between energy and momentum equations is done at the macroscopic level. The convection-diffusion equation of the temperature can be solved with a separate distribution function called s_α in the LB framework. The DBE for the new distribution function is written as

$$\frac{\partial s_\alpha}{\partial t}+\mathbf{e}_\alpha\cdot\nabla s_\alpha=-\frac{1}{\lambda_T}\left(s_\alpha-s_\alpha^{eq}\right), \tag{31}$$

with equilibrium distribution in the form of

$$s_\alpha^{eq}=w_\alpha T\left(1+\frac{\mathbf{e}_\alpha\cdot\mathbf{u}}{c_s^2}\right). \tag{32}$$

It has been shown that the linear equilibrium distribution function, which contains the terms up to first order in $\mathbf{u}$, would be sufficient for solving a typical convection-diffusion equation [21,22]. The DBE of Eq. (31) is integrated along characteristics to achieve LBE for the temperature. Applying the trapezoidal integration leads to

$$s_\alpha(\mathbf{x}+\mathbf{e}_\alpha\delta t,t+\delta t)-s_\alpha(\mathbf{x},t)=-\left.\frac{s_\alpha-s_\alpha^{eq}}{2\tau_T}\right|_{\mathbf{x}+\mathbf{e}_\alpha\delta t,t+\delta t}-\left.\frac{s_\alpha-s_\alpha^{eq}}{2\tau_T}\right|_{\mathbf{x},t}, \tag{33}$$

where $\tau_T=\lambda_T/\delta t$ is the nondimensional relaxation time. Since Eq. (33) is implicit in time, the modified distribution function is introduced as follows to make the scheme explicit with second-order accuracy:

$$\bar{s}_\alpha(\mathbf{x},t)=s_\alpha(\mathbf{x},t)+\frac{s_\alpha(\mathbf{x},t)-s_\alpha^{eq}(\mathbf{x},t)}{2\tau_T}. \tag{34}$$

One can easily derive the LBE for the modified distribution function of temperature as

$$\bar{s}_\alpha(x+e_\alpha\delta t,t+\delta t)-\bar{s}_\alpha(x,t)=-\left.\frac{1}{\tau_T+0.5}\left(\bar{s}_\alpha-\bar{s}_\alpha^{eq}\right)\right|_{(\mathbf{x},t)}. \tag{35}$$

The temperature is calculated by taking the zero-order moment of the above distribution function (i.e., $T=\sum_\alpha s_\alpha=\sum_\alpha \bar{s}_\alpha$) and the thermal diffusion is related to the relaxation time by $\alpha=c_s^2\tau_T\delta t$.

The multiscale Chapman-Enskog expansion of Eq. (35) for recovering the convection-diffusion equation is found extensively in the literature [21–23], but some of the authors have ignored to indicate the errors and unwanted terms recovered by multiscale expansion. Chopard *et al.* [24] discussed the effects of linear and quadratic equilibrium distribution function on the unwanted terms. They showed that with linear equilibrium distribution function, the Chapman-Enskog expansion of Eq. (35) results in

$$\frac{\partial T}{\partial t}+\nabla\cdot(\mathbf{u}T)=\alpha\nabla^2T+\frac{\alpha}{c_s^2}\frac{\partial}{\partial t}\nabla\cdot(\mathbf{u}T), \tag{36}$$

where the last term in the right-hand side is the error term. It is worth noting that the above equation is second-order accurate in time and space as mentioned by Chopard *et al.* [24]. However, neglecting the error term of $\frac{\alpha}{c_s^2}\frac{\partial}{\partial t}\nabla\cdot(\mathbf{u}T)$ needs more justification.

As assumed previously, bulk phases are considered to be incompressible and the compressibility due to the phase change at the interface is mimicked by a proper source term. In the next section we declare another important assumption about the temperature. As we will assume, in this study the liquid phase temperature is fixed at saturation temperature and the energy equation is only solved for the gas phase. Thus, due to incompressibility of the gas phase, the error term of Eq. (36) can be reduced to $\frac{\alpha}{c_s^2}\frac{\partial}{\partial t}\mathbf{u}\cdot\nabla T$. After some algebra, one may find that this unwanted term is of order $O(\frac{\mathbf{u}^2}{c_s^2})$ [25]. Since in incompressible limits the Mach number should be small enough to ensure $\frac{\mathbf{u}}{c_s}\ll 1$, the terms of order $O(\frac{\mathbf{u}^2}{c_s^2})$ could be neglected. Hence, the convection-diffusion equation for temperature can be derived as

$$\frac{\partial T}{\partial t}+\nabla\cdot(\mathbf{u}T)=\alpha\nabla^2T. \tag{37}$$

In this work, the D1Q3 lattice is used for one-dimensional problems and the D2Q9 for two-dimensional simulations for the temperature distribution function ($\bar{s}_\alpha$). For the linear equilibrium distribution function of Eq. (32), the simpler lattice structures such as D2Q4 or D2Q5 can also be employed without the loss of accuracy and stability [25].

D. Computation of the volumetric source due to phase changes

The phase transition from the liquid phase to the gas phase is called vaporization. Evaporation is a type of vaporization which occurs on the liquid surface. From the macroscopic point of view one can assume that the vapor source is present at the phase interface and the gaseous ambience, which is located away from the interface, contains a lower vapor concentration. Thus evaporation can be explained as a continuous diffusion of vapor from the phase interface to the ambience. In this concept the evaporation rate depends on the temperature and the concentration of the different species.

In some practical applications such as droplet heating and evaporating in combustion engines and gas turbines, the

transient heating period does not affect the droplet lifetime considerably [26]. Therefore, for studying the evaporating droplets at enginelike conditions, the droplet is sometimes assumed to be at boiling temperature or saturation temperature. Thus the heat which is transferred from the bulk gaseous phase to the liquid interface causes the vaporization at the phase interface. Moreover this postulation eliminates the necessity of solving the energy equation in the liquid phase and the species concentration transport equation in the gas phase.

In this paper the liquid phase temperature is assumed at saturation temperature and the driving force for evaporation is the amount of heat which is transferred to the interface. So by applying the energy balance for the interface regions the local vaporizing mass flow rate per unit surface ($\dot{m}''$) may be written as

$$\dot{m}'' = \frac{K\nabla T}{h_{fg}} \cdot \hat{\mathbf{n}}, \tag{38}$$

where h_{fg} is the latent heat of vaporization, K is the thermal conductivity, and $\hat{\mathbf{n}}$ is the unit vector normal to the phase interface. The above vaporization rate is computed per unit surface, so it should be converted to the volumetric form in order to be employed in the convective Cahn-Hilliard equation. The interface area at each computational cell or node is needed for calculation of the volumetric mass source or sink. As discussed before, the composition C is similar to the volume-fraction function used in the VOF method. Since our phase-field LB framework is physically a diffuse-interface modeling approach, instead of having an exact interface at which the evaporation takes place, we will have a vaporization region in which the liquid phase evaporates continuously. In this context referring to Hardt and Wondra [27], one important feature of the gradient of the volume-fraction field is that its integral over a region including a part of the phase interface measures the local interface area. This statement is thus valid for the gradient of the composition field (i.e., $\int_V |\nabla C| dV = \int_S dS$). So by multiplying $\dot{m}''$ with the local interface content (i.e., $|\nabla C|$) and recalling $\hat{\mathbf{n}} = \frac{\nabla C}{|\nabla C|}$, the volumetric mass source of evaporation can be obtained as

$$\dot{m}''' = \frac{K\nabla T}{h_{fg}} \cdot \nabla C. \tag{39}$$

In more general situations, the evaporative mass flux is related to the gradient of vapor concentration instead of the gradient of the temperature. The extension of the above mentioned routines to these general cases seems to be straightforward and would be a topic of future work.

III. RESULTS AND DISCUSSION

A. One-dimensional validation tests

The one-dimensional Stefan problem, for which an analytical solution is available, is a well-known benchmark to test two-phase flow phase-change simulations. It was first considered by Son and Dhir [2] for validation of the level set method and later by Welch and Wilson [1] for the VOF method. In the problem, the vapor and liquid phases are initially at a stationary state with saturation temperature. As shown in Fig. 1, the vapor phase is in contact with an isothermal wall. Once the wall experiences an increase in the temperature, heat is transferred to the interface leading the liquid to evaporate. In this flow, the vapor will be motionless while the interface and liquid would be driven away from the wall.

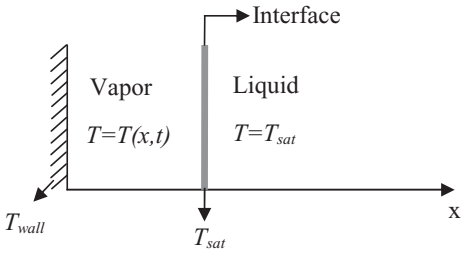

FIG. 1. Schematic view of the one-dimensional Stefan problem.

The temperature equation of the vapor phase can be written as

$$\frac{\partial T}{\partial t} = \alpha \frac{\partial^2 T}{\partial x^2} \quad 0 \leqslant x \leqslant x_i(t), \tag{40}$$

where $x_i(t)$ is the interface location and $\alpha = K_g/(\rho_g c_{p,g})$ is the thermal diffusivity. The boundary conditions are

$$T(x=0,t) = T_{\text{wall}}, \quad T[x=x_i(t),t] = T_{\text{sat}}. \tag{41}$$

The problem is closed by applying a jump condition for the temperature:

$$\rho_g u_i h_{fg} = -K_g \left.\frac{\partial T}{\partial x}\right|_{x=x_i(t)}, \tag{42}$$

in which $u_i = \frac{dx_i}{dt}$ is the interface velocity. The analytical solution for the interface location can be expressed as [1]

$$x_i(t) = 2\beta\sqrt{\alpha t}, \tag{43}$$

where β is the solution to the following transcendental equation:

$$\beta \exp(\beta^2)\text{erf}(\beta) = \frac{c_{p,g}(T_{\text{wall}} - T_{\text{sat}})}{h_{fg}\sqrt{\pi}}. \tag{44}$$

The liquid phase velocity can be obtained by assuming a mass continuity jump condition at the interface:

$$u_l = u_i\left(1 - \frac{\rho_g}{\rho_l}\right). \tag{45}$$

This problem is sometimes rescaled using the dimensionless Stefan number which is defined as the ratio of sensible heat to the latent heat:

$$\text{St} = \frac{c_{p,g}(T_{\text{wall}} - T_{\text{sat}})}{h_{fg}}. \tag{46}$$

A D1Q3 lattice Boltzmann model is developed for the one-dimensional Stefan problem. The left boundary is set as an isothermal wall. The bounce-back rule is applied to the momentum and composition distribution functions ($\bar{g}_\alpha$ and $\bar{h}_\alpha$) (see Appendix), while a constant temperature boundary condition is employed for the temperature distribution function (s_α). The right boundary is considered to be the outflow boundary. A second-order extrapolation is used for the evaluation of unknown distribution functions of the momentum

and composition [23]. Since the temperature of the liquid phase remains constant during the phase-change process, the temperature distribution function in the liquid phase is assumed to be at equilibrium.

In the method of Lee, one needs to compute the second-order central and biased (upwind) differences of the macroscopic variables at each node. For boundary nodes ($\mathbf{x}_b$) and their neighboring nodes ($\mathbf{x}_b - \mathbf{e}_\alpha \delta t$), the information at ($\mathbf{x}_b + \mathbf{e}_\alpha \delta t$) and/or ($\mathbf{x}_b + 2\mathbf{e}_\alpha \delta t$) is required. Lee [20] suggested that when the points ($\mathbf{x}_b + \mathbf{e}_\alpha \delta t$) and ($\mathbf{x}_b + 2\mathbf{e}_\alpha \delta t$) are located outside the computational domain near wall boundaries, the correspondent macroscopic variables are approximated by

$$\begin{aligned} \phi(\mathbf{x}_b + \mathbf{e}_\alpha \delta t) &= \phi(\mathbf{x}_b - \mathbf{e}_\alpha \delta t), \\ \phi(\mathbf{x}_b + 2\mathbf{e}_\alpha \delta t) &= \phi(\mathbf{x}_b - 2\mathbf{e}_\alpha \delta t), \end{aligned} \tag{47}$$

where ϕ can be any variable such as density, pressure, composition, etc. As Lee mentioned [20], Eq. (47) avoids unphysical mass and momentum transfer through the wall boundary nodes.

For open boundaries such as outflow boundary condition two additional virtual nodes are assumed to exist at ($\mathbf{x}_b + \mathbf{e}_\alpha \delta t$) and ($\mathbf{x}_b + 2\mathbf{e}_\alpha \delta t$). These nodes do not take part in the collision and streaming steps and consequently do not have any information about the distribution functions. However, only the information about the macroscopic variables is available for virtual nodes. An extrapolation technique is employed to evaluate the variables at these nodes. Suppose that the node $\mathbf{x}_b$ is located on the open boundary while the nodes $\mathbf{x}_b - \mathbf{e}_\alpha \delta t$ and $\mathbf{x}_b - 2\mathbf{e}_\alpha \delta t$ are inside the domain. A quadratic profile passing these three nodes is determined for the variable ϕ. Assuming this profile to be held at the virtual nodes, the unknown variables can be simply approximated. More details about imposing different boundary conditions are found in the Appendix.

Different density ratios (1:10, 1:100, and 1:1000) are considered to validate the simulations. The thermal diffusivity of the gas phase is set to 2.5×10^{-4} m^2/s for the case of density ratio 10. With the assumption of constant heat conductivity and specific heat capacity, the thermal diffusivity for density ratios 100 and 1000 will be 2.5×10^{-3} m^2/s and 2.5×10^{-2} m^2/s, respectively. The Stefan number is fixed to be 0.02 in all cases. Figures 2 and 3 show the evolution of the interface location and liquid phase velocity for the analytical solutions and simulation results. The lines represent the analytical solutions while the numerical results are indicated by symbols. A grid spacing of $\Delta x = 0.1$ mm is used for numerical simulations. As can be seen, excellent agreement between the numerical and analytical solutions can be obtained. This means that the volumetric source term evaluated by Eq. (39) can satisfactorily account for the phase-change process.

Since a diffuse-interface modeling approach is used in our framework, the interface thickness has noticeable influence on phenomena taking place at the interfacial region. As we reduce the interface thickness, the maximum value of ∇C will increase accordingly. Referring to Eq. (39), the evaporative mass flux is dependent on ∇C. On the other hand, as a result of Eq. (6), the increase of the density ratio will increase the gas volume generated by evaporation. Thus, we found that

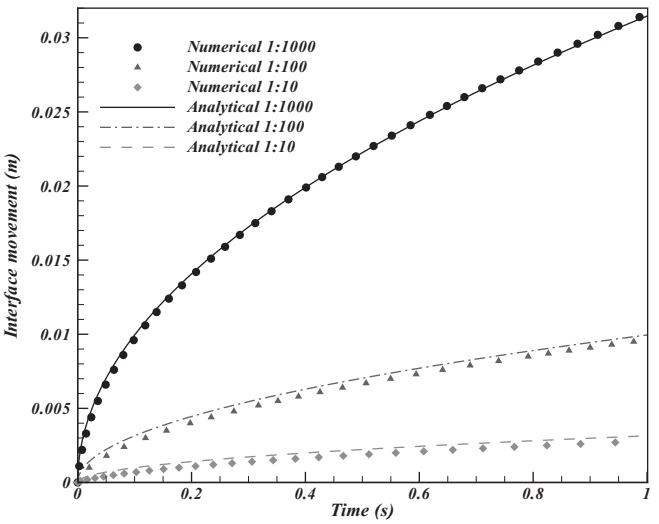

FIG. 2. Comparison between the numerical and analytical solutions of interface location for different density ratios.

as the density ratio increases, the interface thickness should increase in order to decrease the maximum value of ∇C and provide a balance in estimating the evaporation speed. We set the interface thickness as 3, 4, and 5 lattice units for the density ratios of 10, 100, and 1000, respectively.

A convergence study is done for different grid resolutions. The relative global L^2-norm error of the simulated interface location is defined as

$$E_{L^2} = \frac{\sum (x_{\text{numerical}} - x_{\text{analytical}})^2}{\sum (x_{\text{analytical}})^2}, \tag{48}$$

where $\sum$ implies summation over all grid nodes. The L^2-norm error is plotted against the inverse value of grid spacing for three different density ratios in Fig. 4. We observe that essentially quadratic convergence is achieved over the whole range of density ratios.

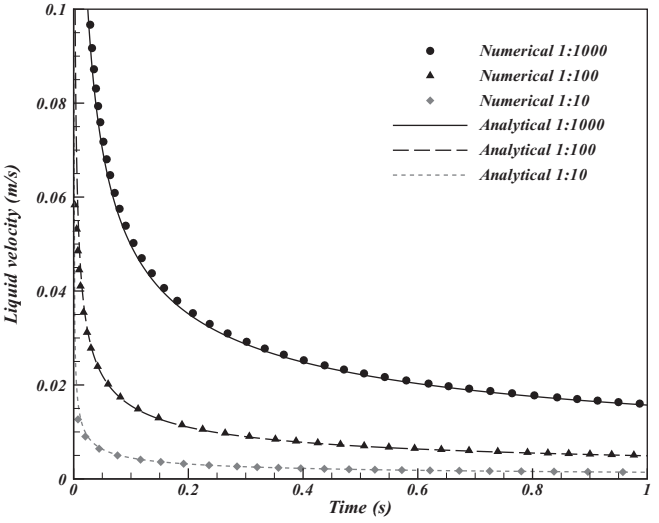

FIG. 3. Comparison between numerical and analytical solutions of liquid phase velocity for different density ratios.

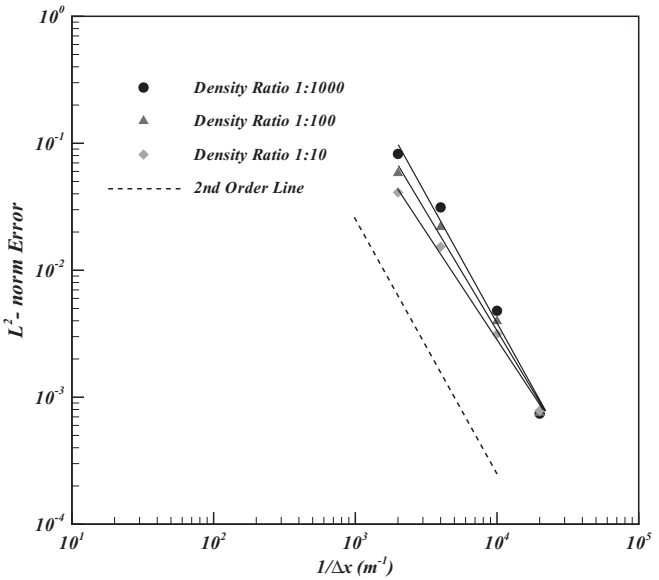

FIG. 4. L^2-norm error of the simulated interface location versus grid size for low to high density ratios.

B. Two-dimensional droplet evaporation

In order to assess the validity of the model for two-dimensional (2D) problems, an isolated static droplet vaporization is selected as a test case. The D2Q9 lattice structure is used for the following simulations. The evaporation is caused by the temperature gradient at the interface. As in the case of the one-dimensional Stefan problem, the liquid phase (droplet) temperature is assumed to be the saturation temperature. The gas phase temperature is kept above the droplet temperature by applying the constant temperature condition on the boundaries. As shown in Fig. 5, due to symmetry with respect to the axis of coordinates, a 2D droplet is initialized at the corner of the computational domain and only a quadrant of the whole domain will be computed. The outflow boundary condition

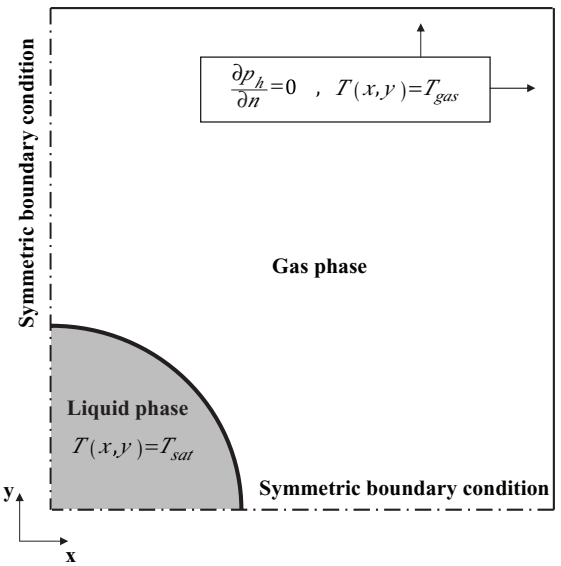

FIG. 5. Schematic representation of the vaporizing droplet simulation.

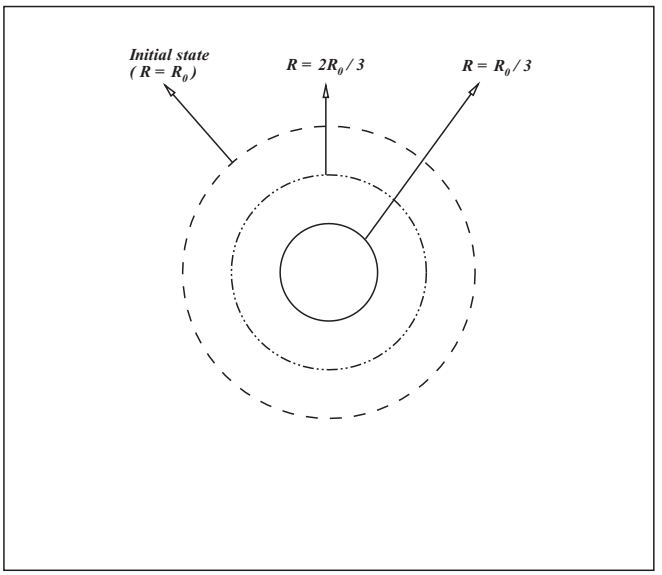

FIG. 6. Droplet interface shape during evaporation for the time steps 0, 130 000, and 260 000. Interface is represented by $C = 0.5$ contour.

is considered by assuming $\frac{\partial p_h}{\partial n} = 0$, where n is the normal direction to the boundary.

At the initial time step, the uniform temperature of T_{gas} is set for the gas phase, while the droplet temperature is fixed to T_{sat}. The existence of the temperature gradient at the phase interface leads to the vaporization of the droplet to the gaseous ambient. As a result of evaporation, a radial velocity profile called Stefan flow should be generated around the droplet in the gas phase, whereas the droplet remains stationary. The simulation is carried out on a 100×100 computational domain discretized by 100×100 grid nodes with an initial droplet radius of $R_0 = 20$. The densities are fixed at $\rho_l = 1.0$ and $\rho_g = 0.001$ (density ratio 1000). The temperature difference $\Delta T = T_{\text{gas}} - T_{\text{sat}}$ and h_{fg} is selected to realize a definite Stefan number. In the following results the Stefan number is fixed to $\text{St} = 0.05$ unless otherwise stated.

Figure 6 shows the variations of droplet size and shape for the time steps 0, 130 000, and 260 000. The Stefan number is set to $\text{St} = 0.2$. It can be seen that the circular shape of the 2D droplet is preserved during the evaporation process. The velocity vectors and contours of velocity magnitude (in lattice units) are presented in Fig. 7 for time step 40 000. The vector's radial direction normal to the interface and rotational symmetry with respect to the center of the droplet are consistently reproduced as expected.

To investigate the effects of latent heat and temperature difference ($T_{\text{gas}} - T_{\text{sat}}$) on the evaporation, the reduced square diameter is plotted against time for various Stefan numbers in Fig. 8. The decrease of latent heat or increase of the temperature difference causes the Stefan number to increase and vice versa. As expected, the increase of Stefan number accelerates the evaporation.

In order to evaluate the 2D numerical solutions quantitatively, two different tests will be carried out. The Laplace law is the basic benchmark test to evaluate correct surface tension effects of multiphase models. Lee's model has already been

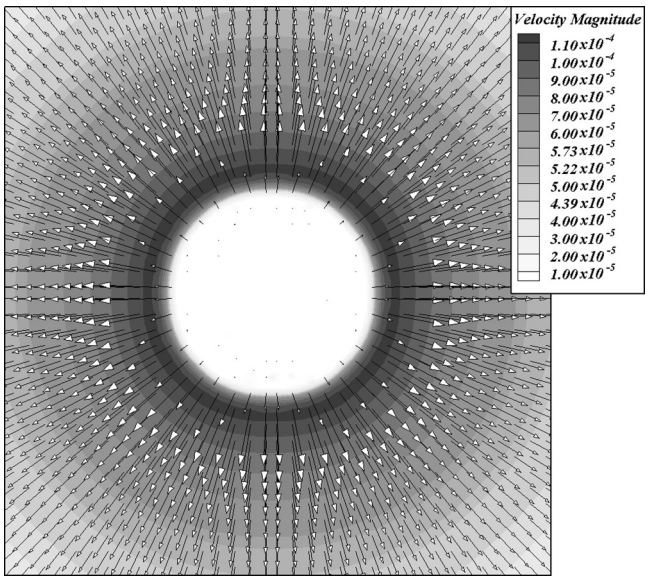

FIG. 7. Velocity vectors and contours of velocity magnitude (in lattice units) at the time step 40 000.

validated for the Laplace test before, but it would be beneficial to check whether our extension to Lee's model will satisfy this law during the vaporization process. Figure 9 represents the pressure difference between the inside and outside of the droplet (ΔP) against $\frac{1}{R}$, where R is the instantaneous droplet radius.

It can be seen that the linear relationship between ΔP and $\frac{1}{R}$ agrees well with theory. However, for a definite instantaneous radius the predicted pressure difference is slightly lower than the exact value. To get more insight about this matter it would be advantageous to declare more details about the conditions of the temperature at the phase interface. Since our multiphase LB model belongs to physical diffuse interface methods, there is no exact and sharp location for physical interface between

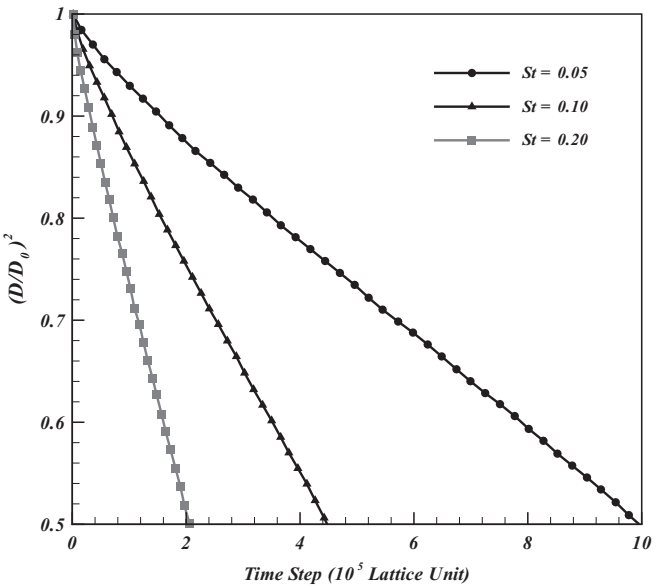

FIG. 8. Reduced square diameter versus time step (D_0 represents the initial drop diameter).

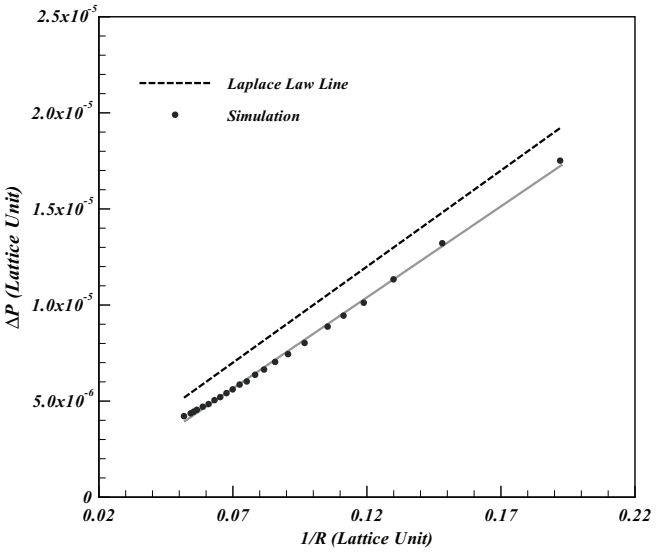

FIG. 9. Laplace law validation during the evaporation process.

the liquid and gas phases. As discussed before, we need to fix the temperature in the liquid phase and the energy equation should be solved only for the gas phase. In order to facilitate meeting this goal, we introduce a cutoff value of the composition C. Each node with the condition of $C \geqslant C_{\text{cutoff}}$ has the liquid temperature of $T = T_{\text{sat}}$ and the related temperature distribution function is set to its local equilibrium value described by Eq. (32). The cutoff value can noticeably affect the evaporative mass flux. Considering Eq. (39), a cutoff value closer to 1.0 makes the evaporative region thicker. Thus, the evaporative mass flux will intensify. Our tests for the one-dimensional Stefan problem reveal that numerical results agree well with analytical solutions by taking $C_{\text{cutoff}} \approx 0.9$. The cutoff values of less than 0.9 will underpredict the evaporation speed. On the other hand, increasing the cutoff value has some effects on the thermodynamic pressure of the liquid phase as depicted in Fig. 10.

According to Lee [17], the thermodynamic pressure is only a function of C. During the simulation of nonevaporative static

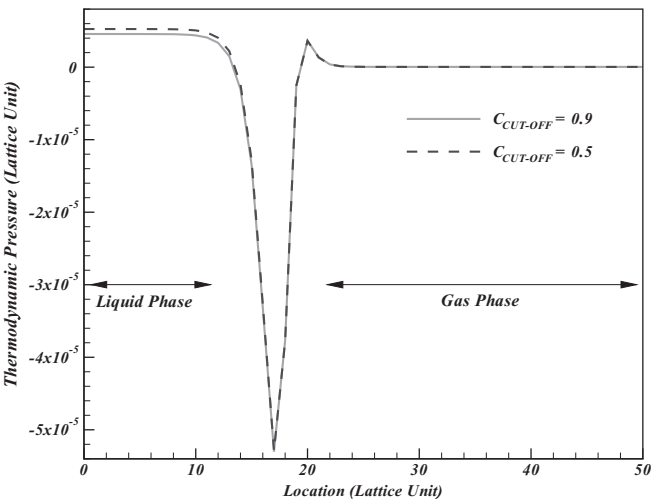

FIG. 10. The effect of the cutoff value on the thermodynamic pressure of each phase.

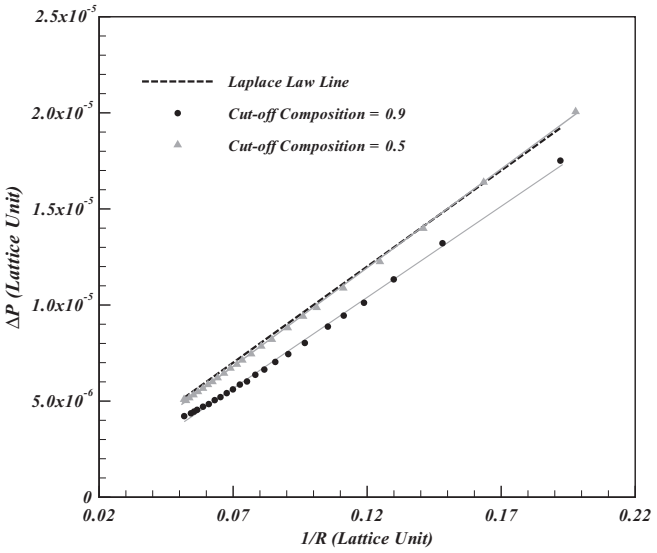

FIG. 11. Comparison between two cutoff values in the Laplace law test during the evaporation process.

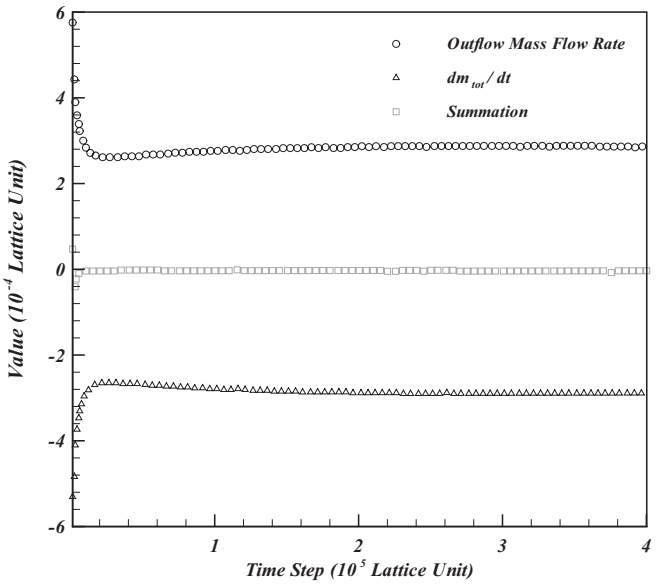

FIG. 12. The total mass conservation test (values are in lattice units).

drop, the maximum and minimum values of the composition C vary a little, so the total pressure (mainly the thermodynamic pressure part) will satisfy the Laplace law. When the evaporation occurs, due to the effects of source terms responsible for the phase change, the values of the composition C in both phases will be changed a bit compared with the nonevaporative case. As we increase the cutoff value, the nodes with larger values of C will be affected by the evaporative source term and their composition value will decrease consequently. Hence, the thermodynamic pressure in the liquid phase varies slightly while the gas phase pressure remains unchanged and the total pressure difference between the two phases deviates from equilibrium Laplace pressure. The effect of cutoff value on the Laplace law test is also shown in Fig. 11 and Table I.

As another test we check the total mass conservation within the computational domain, as a reliable numerical scheme for computational fluid dynamics (CFD) should be mass conservative. In our case, as a result of evaporation, the total fluid mass of the computational domain is decreased and the Stefan flow around the droplet initiates a gas flux out of the domain across the outflow boundaries. In order to perform a mass conservation test, two different terms are calculated during the evaporation; the time derivative of the total fluid mass of the computational domain ($\frac{dm_{\text{tot}}}{dt}$) and the gas flow rate across the outflow boundaries. Mass conservation requires that these two terms cancel each other and their summation should be zero. Figure 12 represents the variations of these terms over different time steps. The approximate satisfaction of the mass conservation law can be observed from the curves. The results demonstrate an acceptable accuracy to predict the behavior of a complicated problem such as evaporation. The sharp slopes of the diagrams at early time steps are due to the high temperature gradients near the phase interface. After a few time steps the temperature gradient is smoothed because of heat diffusion and a nearly constant evaporation rate is achieved.

Figure 12 confirms that the employed phase-change model and the implemented boundary conditions do not lead to any mass accumulation or mass disappearance within the computational domain. In other words, the evaporated mass within the interface region generates a consistent mass flux at the outlet boundaries of the domain.

IV. CONCLUSION

In this article, a method has been proposed to simulate phase-change effects based on the LBM multiphase model of Lee. The convective Cahn-Hilliard equation which is responsible for phase separation was extended to reflect phase transition effects. A suitable source term was also added to the

TABLE I. The effect of the composition cutoff value on satisfaction of the Laplace law. The surface tension is fixed to 1.00×10^{-4}. All values are in lattice units.

$\frac{1}{R}$	ΔP (Laplace law)	ΔP ($C_{\text{cutoff}} = 0.5$)	ΔP ($C_{\text{cutoff}} = 0.9$)	Relative error (%) ($C_{\text{cutoff}} = 0.5$)	Relative error (%) ($C_{\text{cutoff}} = 0.9$)
0.05	5.00×10^{-6}	4.92×10^{-6}	4.49×10^{-6}	1.66	10.26
0.075	7.50×10^{-6}	7.28×10^{-6}	6.58×10^{-6}	2.92	12.23
0.10	1.00×10^{-5}	9.78×10^{-6}	8.90×10^{-6}	2.23	10.98
0.15	1.50×10^{-5}	1.49×10^{-5}	1.32×10^{-5}	0.44	11.90
0.175	1.75×10^{-5}	1.77×10^{-5}	1.54×10^{-5}	1.11	12.02
0.19	1.90×10^{-5}	1.94×10^{-5}	1.66×10^{-5}	2.11	12.70

pressure-momentum distribution function to take into account the effects of phase-change phenomena on the velocity field. In order to calculate the volumetric source due to the phase change within the interface region, the passive scalar thermal lattice Boltzmann framework was successfully combined with the multiphase LBM model. Different tests were carried out for one- and two-dimensional cases to validate the approach and demonstrate the consistency of the results.

Our approach explains the vaporization macroscopically with the aid of appropriate physical postulations: Vaporization can be described as the change of phase composition (C) with a rate proportional to the temperature or vapor species concentration gradient at the interface. One of the most important features of this approach is the ease of implementation. The divergence of the velocity field ($\nabla \cdot \mathbf{u}$) is evaluated globally on each node by Eq. (6) and there is no need to apply any special jump conditions at the interface to explain the mass and momentum transfer between two phases. This will substantially simplify the simulations of more complex cases such as problems involving porous media or situations with a strong degree of interface deformation.

Future works will focus on more general situations in which the evaporation is forced by vapor concentration gradient rather than temperature gradient. Moreover, it would be interesting to include partial wetting wall boundary conditions in the model to study more challenging real world problems such as substrate evaporation and evaporation within three-dimensional porous media.

APPENDIX

In this Appendix, different boundary conditions used in our simulations are briefly discussed. Since $\bar{g}_\alpha$ and $\bar{h}_\alpha$ [Eqs. (21) and (26)] contain forcing terms, in general the bounce-back rule should be applied to g_α and h_α (not $\bar{g}_\alpha$ and $\bar{h}_\alpha$), because reflecting the force terms back to the domain seems unphysical. The nonslip condition for the wall causes zero velocity ($\mathbf{u} = 0$) at the wall boundary node $\mathbf{x}_b$. Thus, only directional derivatives $[\mathbf{e}_\alpha \cdot \nabla()]$ contribute to the forcing terms on the right-hand side of Eqs. (21) and (26). According to Lee [20], these derivatives should be discretized by employing the central difference approximation. Recalling Eq. (47), one can easily obtain that the directional derivatives in every direction except the directions along the wall will go to zero. For example, in the D2Q9 lattice for the left wall we have $\mathbf{e}_\alpha \cdot \nabla() = 0$, where $\alpha = 1,3,5,6,7,8$. Hence, the forcing terms on the solid wall are canceled out in the bounce-back directions. For directions in which the bounce back is applied, the modified distribution functions can be written as

$$\bar{z}_\alpha = z_\alpha + \frac{\left(z_\alpha - z_\alpha^{eq}\right)}{2\tau}, \tag{A1}$$

where z can be either g or h. As $\mathbf{u} = 0$ at $\mathbf{x}_b$, $z_\alpha^{eq}(\mathbf{x}_b) = z_{\bar{\alpha}}^{eq}(\mathbf{x}_b)$, where $\bar{\alpha}$ is in the opposite direction of α. So it can be concluded from Eq. (A1) that we can apply the bounce-back rule on $\bar{g}_\alpha$ and $\bar{h}_\alpha$ instead of g_α and h_α.

The constant temperature boundary condition is applied similarly to that proposed by Inamuro *et al.* [22]. In this approach, the unknown distribution functions are assumed to be the equilibrium distribution functions calculated by Eq. (32) with an unknown parameter T' as

$$\bar{s}_\alpha|_{\text{unknown}} = w_\alpha T' \left(1 + \frac{\mathbf{e}_a \cdot \mathbf{u}_b}{c_s^2}\right), \tag{A2}$$

where $\mathbf{u}_b$ is the velocity of the boundary. The unknown parameter T' is determined so that the constant temperature of T_b is satisfied on the boundary;

$$\sum_\alpha \bar{s}_\alpha = \sum_{\text{unknown}} w_\alpha T' \left(1 + \frac{\mathbf{e}_a \cdot \mathbf{u}_b}{c_s^2}\right) + \sum_{\text{known}} \bar{s}_\alpha = T_b. \tag{A3}$$

Once the parameter T' is determined by Eq. (A3), the unknown distribution functions are computed by Eq. (A2).

The unknown distribution functions of the composition ($\bar{h}_\alpha$) are approximated by the second-order extrapolation as described in [23]:

$$\bar{h}_\alpha(\mathbf{x}_b) = 2\bar{h}_\alpha(\mathbf{x}_b - \mathbf{e}_\alpha \delta t) - \bar{h}_\alpha(\mathbf{x}_b - 2\mathbf{e}_\alpha \delta t). \tag{A4}$$

In order to apply the condition of $\frac{\partial p_h}{\partial n} = 0$ on the outflow boundaries, the hydrodynamic pressure on the boundary is calculated by the second-order backward difference as

$$p_{h,b} = p_h(\mathbf{x}_b) = \frac{4p_h(\mathbf{x}_b - \mathbf{e}_n \delta t) - p_h(\mathbf{x}_b - 2\mathbf{e}_n \delta t)}{3}. \tag{A5}$$

Then, an approach similar to the one described for the temperature can be employed for the pressure. The unknown pressure-momentum distribution functions are assumed to be the equilibrium ones. Combining Eqs. (19) and (22), $\bar{g}_\alpha^{eq}$ is written as

$$\bar{g}_\alpha^{eq} = p_h \Gamma_\alpha(0) + \rho c_s^2 [\Gamma_\alpha - \Gamma_\alpha(0)] - \frac{\delta t}{2}(\mathbf{e}_\alpha - \mathbf{u}) \cdot \left\{\nabla \rho c_s^2 [\Gamma_\alpha - \Gamma_\alpha(0)] - C \nabla \mu \Gamma_\alpha\right\}. \tag{A6}$$

The hydrodynamic pressure (p_h) is replaced with an unknown parameter (p_h') for calculation of the unknown distribution functions. From Eq. (30), the unknown distribution functions can be evaluated by

$$\sum_\alpha \bar{g}_\alpha = \sum_{\text{unknown}} \bar{g}_\alpha + \sum_{\text{known}} \bar{g}_\alpha = p_{h,b} - \frac{\delta t}{2} \mathbf{u} \cdot \nabla \rho c_s^2, \tag{A7}$$

in which $\sum_{\text{unknown}} \bar{g}_\alpha$ is approximated by $\sum_{\text{unknown}} \bar{g}_\alpha^{eq}$. Notice that due to the presence of the velocity ($\mathbf{u}$) in the right-hand side of Eq. (A7), an iteration process should be employed for evaluating the unknown parameter p_h'.

[1] S. W. J. Welch and J. Wilson, J. Comput. Phys. **160**, 662 (2000).

[2] G. Son and V. K. Dhir, J. Heat Transfer **121**, 623 (1999).

[3] D. Juric and G. Tryggvason, Int. J. Multiphase Flow **24**, 387 (1998).

[4] T. Inamuro, T. Ogata, S. Tajima, and N. Konishi, J. Comput. Phys. **198**, 628 (2004).

[5] T. Lee and C.-L. Lin, J. Comput. Phys. **206**, 16 (2005).

[6] T. Lee and P. F. Fischer, Phys. Rev. E **74**, 046709 (2006).

[7] B. J. Palmer and D. R. Rector, Phys. Rev. E **61**, 5295 (2000).
[8] M. R. Swift, E. Orlandini, W. R. Osborn, and J. M. Yeomans, Phys. Rev. E **54**, 5041 (1996).
[9] B. J. Palmer and D. R. Rector, Phys. Rev. E **69**, 049903(E) (2004).
[10] T. Lee and C.-L. Lin, Phys. Rev. E **67**, 056703 (2003).
[11] R. Zhang and H. Chen, Phys. Rev. E **67**, 066711 (2003).
[12] Z. Dong, W. Li, and Y. Song, Numer. Heat Transfer, Part A **55**, 381 (2009).
[13] H. W. Zheng, C. Shu, and Y. T. Chew, J. Comput. Phys. **218**, 353 (2006).
[14] A. Fakhari and M. H. Rahimian, Phys. Rev. E **81**, 036707 (2010).
[15] Z. Dong, W. Li, and Y. Song, Int. J. Heat Mass Transfer **53**, 4908 (2010).
[16] A. Márkus and G. Házi, Phys. Rev. E **83**, 046705 (2011).
[17] T. Lee, Comput. Math. Appl. **58**, 987 (2009).
[18] Q. Li, K. H. Luo, Y. J. Gao, and Y. L. He, Phys. Rev. E **85**, 026704 (2012).
[19] H. Ding, P. D. M. Spelt, and C. Shu, J. Comput. Phys. **226**, 2078 (2007).
[20] T. Lee and L. Liu, J. Comput. Phys. **229**, 8045 (2010).
[21] Z. Guo, B. Shi, and C. Zheng, Int. J. Numer. Methods Fluids **39**, 325 (2002).
[22] T. Inamuro, M. Yoshino, H. Inoue, R. Mizuno, and F. Ogino, J. Comput. Phys. **179**, 201 (2002).
[23] A. A. Mohamad, *Lattice Boltzmann Method, Fundamentals and Engineering Applications with Computer Codes* (Springer, London, 2011).
[24] B. Chopard, J. L. Falcone, and J. Latt, Eur. Phys. J.: Spec. Top. **171**, 245 (2009).
[25] H.-B. Huang, X.-Y. Lu, and M. C. Sukop, J. Phys. A **44**, 055001 (2011).
[26] F. Mashayek, Int. J. Heat Mass Transfer **44**, 1517 (2001).
[27] S. Hardt and F. Wondra, J. Comput. Phys. **227**, 5871 (2008).